The influence of bearing stiffness on the vibration properties of statically overdetermined gearboxes

M. Razpotnik, T. Bischof [a], M. Boltežar*

Faculty of Mechanical Engineering, University of Ljubljana, Aškerčeva 6, 1000 Ljubljana, Slovenia

[a] Affiliation: ZF Friedrichshafen AG

Abstract

In the design process of every modern car, the appropriate acoustic behaviour of each integral part is of great importance. This is particularly so for gearboxes. The stiffness of a rolling-element bearing is one of the main contributors to the transmission of vibrations from the interior of the gearbox to the housing. Many methods have been proposed to determine the bearing stiffness; this stiffness is related to the load in a nonlinear way. In this article, a new method for defining the proper bearing stiffness of statically overdetermined gearboxes is proposed. To achieve this an iterative process is conducted, with an initial guess for the loads on the bearings, which provides the initial values for their stiffnesses. The calculated stiffnesses are then inserted into a finite element method (FEM) model of a gearbox, where the new load vectors on the bearings are calculated. The described process runs until the convergence of the loads on the bearings is reached. Afterwards, the frequency-response functions (FRFs) are numerically calculated. As a reference point for our calculations, the measured FRFs are obtained. The measurements were performed on a simple, but statically overdetermined, gearbox with the option for moment adjustments between the two shafts. The calculated results in the form of FRFs are compared with the measurements.

1. Introduction

The transmission of vibrations through bearings is a major topic of interest with respect to rotating machinery. Over the past few decades, many approaches and results have been presented in the field of bearing models and the transmission of vibrations through bearings. In order to predict the proper dynamic response of a known system, the correct bearing-stiffness matrices need to be obtained. We will present an approach for obtaining the proper bearing-stiffness matrices for statically overdetermined gearboxes.

Bearing models that prescribe their dynamics were already investigated in the past and remain a major issue nowadays. The first bearing models represented the bearings as the ideal boundary conditions for the shaft [1, 2]. Meanwhile, the idea of interpreting the bearings with a simple one- or two-degree-of-freedom (DOFs) model, with linear springs including damping mechanisms, was introduced [3–6]. Later, more precise bearing models were deduced, taking more degrees of freedom into account. The main improvement was the five-DOFs bearing model [7], which properly describes the nonlinear behaviour between the load and the deflection. This particular model was the basis for many subsequent investigations [8], including ours. The same authors extended their investigation of vibration transmission through rolling-element bearings to geared-rotor-system studies [9] and additionally provided a statistical energy analysis [10]. Later, an indirect approach to define the bearing stiffness was conducted [11] as well as an investigation of the time-varying rolling-element characteristics [12] and the effect of bearing preloads on the modal characteristics of a shaft-bearing assembly [13]. In recent years new techniques for defining the proper dynamic bearing parameters have appeared with use of the FEM models. A stiffness matrix of rolling-element bearings was calculated using a finite-element/contact-mechanics model in [14]. The authors precisely modelled each part of the bearing and implemented a special contact model [15] between the rolling elements and the raceways. The time-dependent characteristics of the bearing contact due to the orbital motion of the rolling elements were captured and the stiffness determination method was compared to the existing analytical models in the literature. Recently, the bearing speed-varying stiffness has been studied and explained analytically [16].

*Corresponding author. Tel.: +386-1-4771-608; fax: +386-1-2518-567.
E-mail address: miha.boltezar@fs.uni-lj.si (M. Boltežar).

The experimental approach to obtaining the bearing-stiffness matrix and damping has been to a large extent limited to the translational coefficients. An experimental modal analysis to estimate the modal parameters of a shaft-bearing system using a single-DOF system was utilized [17], with the experiment being performed in the axial and transverse directions. The transmission of vibrations through self-aligning, (spherical) rolling-element bearings, where some of the terms from the stiffness matrix were validated experimentally, was studied in [8], while in [18, 19] experimental results were also presented. The authors loaded the bearings axially, with three different preloads, but did not observe a relation between the bearing preloads and the vibration amplitudes. The bearing-stiffness changes due to the high rotational speed were studied and measured in [20]. Recently, experimental results of the influence of the lubricant film on the bearing stiffness and damping characteristics [21] were reported.

So far studies have been limited to statically determined gearboxes with rolling-element bearings, while the recent work in [22] might, in addition, handle the statically overdetermined systems as well, but at the expense of an enormous computational time due to the finite-element/contact-mechanics model incorporated into the calculation procedure. The aforementioned study was not meant to calculate statically overdetermined systems, but the vibration properties of the gearbox in operational conditions, i.e., while the shafts rotate at a certain load. One approach to dealing with statically overdetermined systems was conducted in [23], where the authors compared different techniques for identifying the configuration state of statically overdetermined rotor-bearing systems; they investigated hydrodynamic bearings and tribological effects.

In this article the influence of bearing stiffness on the vibration properties of statically overdetermined gearboxes is presented. Different types of rolling-element bearings are implemented and measurements of the FRFs between the different parts of the gearbox are conducted. An algorithm for the FEM model updating together with a bearing-stiffness calculation are developed in order to solve the problem of overdetermination. Different loads are applied (numerically and experimentally) to check the influence of a nonlinear bearing-stiffness change on the FRFs. Finally, a comparison is made between the experimental results and the results of the new algorithm.

2. The bearing model

The bearing model used in this investigation was developed by Lim and Singh [7]. For the sake of clarity, let us present the basic steps in its derivation. Following Figure 1, the *bearing mean-load* vector, $\mathbf{F}_{bm}$, and the *bearing mean-displacement* vector, $\mathbf{q}_{bm}$, are defined as:

$$\mathbf{F}_{bm} = \{F_{xbm}, F_{ybm}, F_{zbm}, M_{xbm}, M_{ybm}\}^{\mathrm{T}}, \tag{1}$$

and

$$\mathbf{q}_{bm} = \{\delta_{xbm}, \delta_{ybm}, \delta_{zbm}, \beta_{xbm}, \beta_{ybm}\}^{\mathrm{T}}, \tag{2}$$

where F are forces in N, M are moments in N m, δ are displacements in m and β are rotations in rad. For the jth rolling element we can express the normal, δ_{n_j}, and the radial, δ_{r_j}, displacements as:

$$\delta_{n_j} = \delta_{zbm} + r_j(\beta_{xbm}\sin\psi_j - \beta_{ybm}\cos\psi_j), \tag{3}$$

and

$$\delta_{r_j} = \delta_{xbm}\cos\psi_j + \delta_{ybm}\sin\psi_j - r_c, \tag{4}$$

where r_j is the radial distance of the inner-raceway groove-curvature centre for the ball type or is the pitch bearing radius for the roller type. r_c represents the radial clearance. The contact angle α_j for ball bearings (see Figure 2) is defined as:

$$\tan\alpha_j = \frac{\delta^*_{n_j}}{\delta^*_{r_j}}, \qquad \delta^*_{n_j} = A_0\sin\alpha_0 + \delta_{n_j}, \qquad \delta^*_{r_j} = A_0\cos\alpha_0 + \delta_{r_j}, \tag{5}$$

whereas $\alpha_j = \alpha_0$ for roller bearings. In Equation (5) A_0 represents the unloaded distance between the inner- and outer-raceway groove-curvature centres, and α_0 is the unloaded bearing contact angle. $\delta^*_{r_j}$ and $\delta^*_{n_j}$ are the rolling-element displacements in the radial and normal (axial) directions from the outer-raceway groove-curvature centre. The loaded distance between the inner- and outer-raceway curvature centres for the ball bearings is expressed as:

$$A(\psi_j) = \sqrt{(\delta^*_{r_j})^2 + (\delta^*_{n_j})^2}, \tag{6}$$

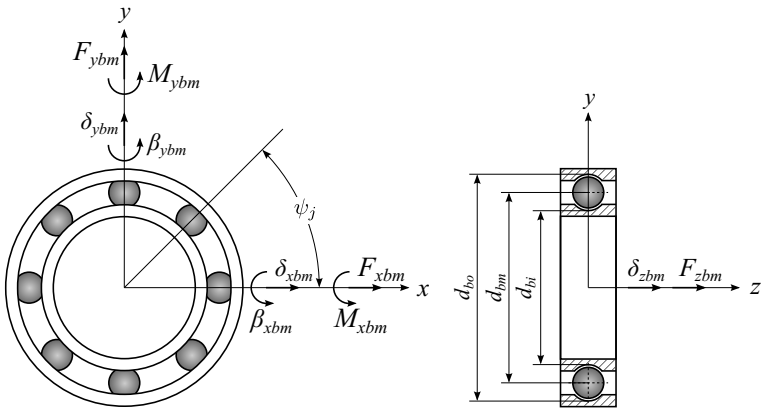

Figure 1: Deep-groove ball bearing with dimensions, mean loads and mean displacements.

and from the ball- and roller-bearing kinematics, shown in Figure 2, is the resultant elastic deformation of the jth ball element $\delta_B(\psi_j)$ and the resultant elastic deformation of the jth roller element $\delta_R(\psi_j)$, defined as:

$$\delta_B(\psi_j) = \begin{cases} A(\psi_j) - A_0, & \delta_{B_j} > 0 \\ 0, & \delta_{B_j} \leq 0 \end{cases}, \qquad \delta_R(\psi_j) = \begin{cases} \delta_{r_j} \cos\alpha_j + \delta_{n_j} \sin\alpha_j, & \delta_{R_j} > 0 \\ 0, & \delta_{R_j} \leq 0 \end{cases}. \tag{7}$$

Following the Hertzian contact stress principle [5, 6] as $Q_j = K_n \delta_j^n$ (n is equal to $^3/_2$ for ball type

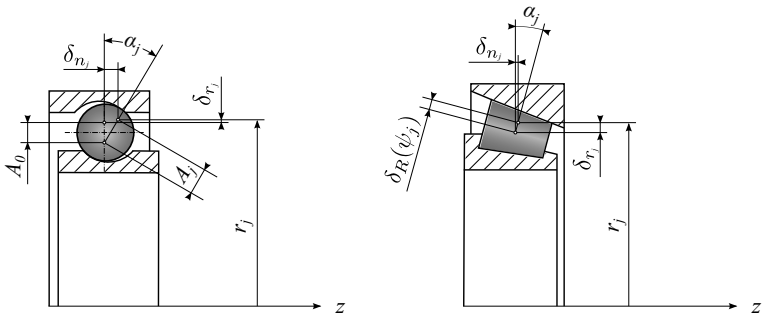

Figure 2: Elastic deformation of rolling element for non constant contact angle α_j (left) and for constant contact angle $\alpha_j = \alpha_0$ (right).

and $^{10}/_9$ for a roller type) we can connect the resultant bearing mean-load vector $\mathbf{F}_{bm}$ to the bearing mean-displacement vector $\mathbf{q}_{bm}$. The bearing mean-load vector is obtained by summing the contribution from z rolling elements:

$$\mathbf{F}_{bm} = \begin{Bmatrix} F_{xbm} \\ F_{ybm} \\ F_{zbm} \\ M_{xbm} \\ M_{ybm} \end{Bmatrix} = \begin{Bmatrix} \sum_{j=1}^{z} Q_j \cos\alpha_j \cos\psi_j \\ \sum_{j=1}^{z} Q_j \cos\alpha_j \sin\psi_j \\ \sum_{j=1}^{z} Q_j \sin\alpha_j \\ \sum_{j=1}^{z} r_j\, Q_j \sin\alpha_j \sin\psi_j \\ -\sum_{j=1}^{z} r_j\, Q_j \sin\alpha_j \cos\psi_j \end{Bmatrix}. \tag{8}$$

Finally, the symmetric bearing-stiffness matrix of dimension five is expressed as:

$$\mathbf{K}_{bm} = \frac{\partial\, \mathbf{F}_{bm}}{\partial\, \mathbf{q}_{bm}} = \begin{bmatrix} k_{xx} & k_{xy} & k_{xz} & k_{x\beta_x} & k_{x\beta_y} \\ & k_{yy} & k_{yz} & k_{y\beta_x} & k_{y\beta_y} \\ & & k_{zz} & k_{z\beta_x} & k_{z\beta_y} \\ & \text{symmetric} & & k_{\beta_x\beta_x} & k_{\beta_x\beta_y} \\ & & & & k_{\beta_y\beta_y} \end{bmatrix}. \tag{9}$$

Equation (9) consists of 15 different stiffness coefficients, nonlinearly dependent on the bearing mean-displacement vector, e.g., for k_{xx} we can write:

$$k_{xx} = K_n \sum_{j=1}^{z} \frac{(A_j - A_0)^n \cos^2 \psi_j \left(\dfrac{n\, A_j\, (\delta^*_{r_j})^2}{A_j - A_0} + A_j^2 - (\delta^*_{r_j})^2 \right)}{A_j^3}. \tag{10}$$

Giving the bearing mean-load vector, the bearing mean-displacement vector can be calculated. This step requires solving a system of five nonlinear equations for each bearing. To achieve this, the Newton-Raphson method (NRM) was implemented. It is important to note that the convergence and stability of the NRM is strongly affected by the initial guess. Section 6 provides more information about this phenomenon. Having the bearing mean-displacement vector, the bearing-stiffness matrix can be obtained directly.

3. Statically overdetermined systems

In statics, a structure is statically indeterminate when the static equilibrium equations are insufficient to determine the reactions and internal forces on that structure. A statically indeterminate system can be either underdetermined or overdetermined. When a system reflects the same number of equations as the number of unknowns, the system is determined.

In this article we are dealing with statically overdetermined systems, which means that the number of static equations is insufficient to solve the problem. Figure 3 illustrates the difference between a statically determined and a statically overdetermined system. A shaft, supported by two equal bearings, loaded with a radial force, positioned in the middle, between both bearings, causes each of the two bearings to feel the corresponding half of the applied force. When investigating such a statically overdetermined

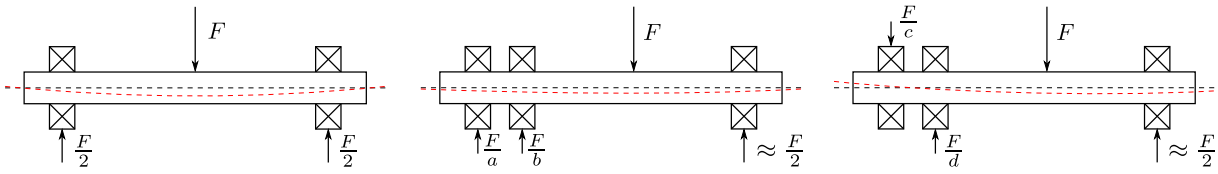

Figure 3: Load distribution on the bearings, representing the forces in vertical direction. Statically determined system (left), statically overdetermined systems (centre and right).

system, the load distribution on the bearings is not so evident any more. Figure 3 illustrates the problem. The values of the parameters in the denominators, a, b, c and d, are initially unknown and are a function of the bearing stiffness, the shaft stiffness and the housing stiffness. It is important to note that Figure 3 shows only the applied and resultant forces in the vertical direction. Investigating the presented load, some moments on the bearings will also appear. However, to present the static overdetermination, let us focus only on the forces in the vertical direction. Having a very stiff shaft and a weak housing, or a very flexible shaft and a stiff housing, means the system will react completely different bearing mean-load vectors. Additionally, the bearing mean-load vector is a function of the bearing stiffness, the shaft stiffness as well as the housing stiffness. For each bearing mean-load vector we can write:

$$\mathbf{F}_{bm} = \mathbf{F}_{bm}(\mathbf{K}_{bm}, \mathbf{K}_{sm}, \mathbf{K}_{hm}). \tag{11}$$

Furthermore, the bearing mean-load vector is nonlinearly dependent on the bearing mean-displacement vector through the governing equation:

$$\mathbf{F}_{bm} = \mathbf{K}_{bm}\, \mathbf{q}_{bm}, \tag{12}$$

as described in Section 2. Consequently, the bearing-stiffness matrix is a function of the bearing mean-load vector:

$$\mathbf{K}_{bm} = \mathbf{K}_{bm}(\mathbf{F}_{bm}). \tag{13}$$

In reality, every statically overdetermined system exhibits one solution, that is the result of an interplay of physical parameters, mainly the stiffness. The stiffnesses of the shaft and the housing are obtained from the geometrical and material properties of the particular parts. On one hand, the bearing-stiffness

matrix can only be obtained after knowing the exact bearing mean-load vector (Equation (13)). On the other hand, the bearing mean-load vector can be obtained after knowing the exact bearing-stiffness matrix, together with the shaft and housing stiffnesses (Equation (11)). One of them is needed in order to obtain the other one. Thus, an initial guess has to be made for one of them. Usually, it is much easier to provide a better initial guess for the bearing mean-load vector. Afterwards, the corresponding bearing-stiffness matrix is calculated. An iterative process has to be implemented in order to find the equilibrium between the two quantities. Defining the correct bearing-stiffness matrices of a statically overdetermined gearbox is one of the main issues in predicting the proper acoustic quality of a gearbox.

4. The gearbox

For the purposes of our investigation we chose a simple, but statically overdetermined, gearbox to investigate the influence of the bearing stiffness on the vibration properties of the entire gearbox. A schematic representation is shown in Figure 4, and a photograph of the real test bench is shown in Figure 5. Our gearbox consists of two main parts, i.e., the test gearbox and the transmission gearbox, both with separate housings and a helical gear pair inside. The gear pairs are connected from one housing

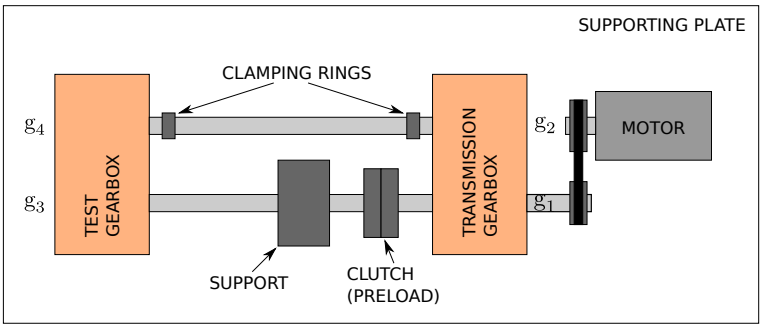

Figure 4: Schematic representation of the chosen statically overdetermined gearbox.

to the other with shafts. The shafts are supported by the bearings in both housings. The whole setup is connected in a loop. The role of the motor is to compensate for losses due to the friction when the system is rotating. The motor is connected to the system with a rubber belt so as to avoid the transmission of vibrations from the motor to the drive shaft. It is important to note that the motor is not rotating when

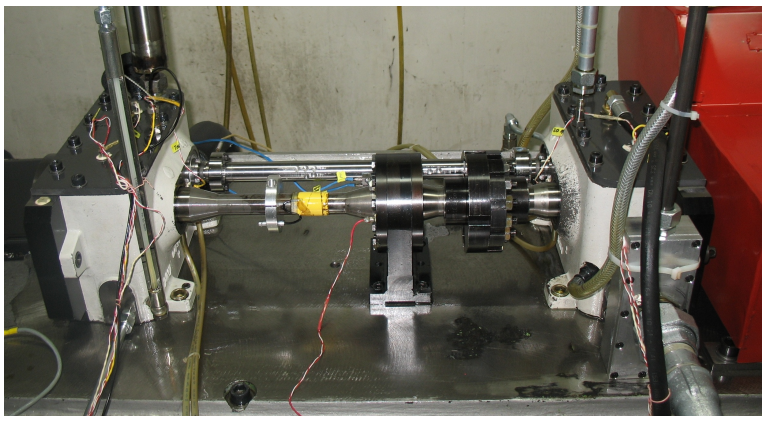

Figure 5: The test bench of the chosen statically overdetermined gearbox.

the measurements are being made. g_1, g_2, g_3, and g_4 are the names of the gears at the marked positions. The data relating to the gear pairs are listed in Table 1. The test gearbox and the transmission gearbox are connected by shafts. One of them is cut into two parts, resulting the shaft w1 and w3, between which a special clutch is attached (see figure 6). The purpose of employing such a clutch is to have the ability to apply different torque preloads in the system. To prevent any axial non-collinearity after changing the torque preload we introduced a special additional support on the section of the shaft where the clutch

is located. Another shaft, which does not have a clutch, is logically one shaft (named w3), but it is made out of three parts (see Figure 6). Two solid parts, where the gears are mounted in the test and transmission gearboxes, and a hollow shaft in the middle, rigidly joined to both of the solid parts by special clamping rings. Everything is set together on the steel supporting plate. It is important to note that the investigated test-bench gearbox was originally made for high-speed applications. Thus, the entire assembly is designed and built up with a high level of accuracy. This is necessary in our investigation, since a slight misalignment could cause significant differences in the bearing loads. However, in reality some degree of misalignment can never be completely removed, but we expect that in our case the slight misalignment interplays with the clearance of the bearings, without really loading them.

Table 1: Gear pairs data.

	module	center distance	number of teeth	gear width	gear ratio	pressure angle	helix angle
gear pair	m [mm]	a [mm]	z	b [mm]	i	α	β
$g_1 - g_2$ $g_3 - g_4$	2.2179	91.5	62 – 16	44.82	3.875	17° 30’	20°

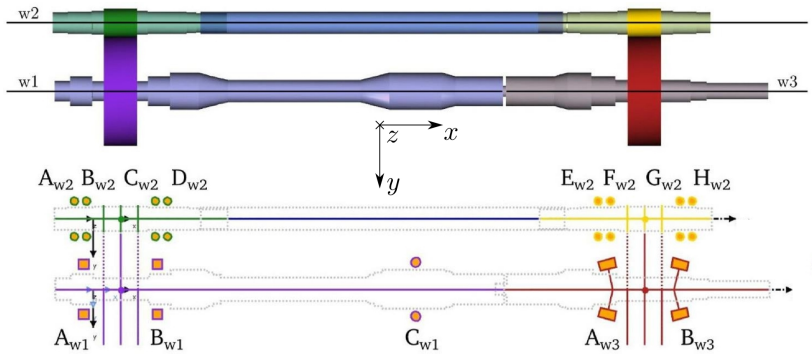

Figure 6: Schematic presentation of the gearbox interior with names of the shafts, bearing names, types and positions.

Due to the number of bearings in our gearbox and their distribution, we are dealing with a statically overdetermined system. Figure 6 schematically shows the shape of the shafts and the connections between all the interior parts of the gearbox, as well as the bearing positions, their types and names. All the bearing types and the description can be found in Table 2. It is clear, that thirteen bearings of four different types are implemented in our gearbox, causing the system to be statically overdetermined.

Table 2: Bearing data.

Bearing name	Bearing type	Bearing code
A_{w1}	roller	NU 308 E/J
B_{w1}	roller	NU 308 E/J
C_{w1}	four-point-contact ball	QJ210N/J
A_{w2}	angular-contact ball	6206
B_{w2}	angular-contact ball	6206
C_{w2}	angular-contact ball	6206
D_{w2}	angular-contact ball	6206
E_{w2}	angular-contact ball	6206
F_{w2}	angular-contact ball	6206
G_{w2}	angular-contact ball	6206
H_{w2}	angular-contact ball	6206
A_{w3}	tapered roller	30308A
B_{w3}	tapered roller	30308A

5. The FEM model

Figure 7 shows the general appearance of the gearbox FEM model used in this study. It is important to note the simplifications made to the gearbox FEM model in comparison with the real gearbox. The electric motor is not modelled, since it is dynamically uncoupled from the system with a rubber belt. The oil and air pipes, mounted on the top lid of both housings, are also excluded from the FEM model, since we expect them to have a negligible influence on the dynamics of the entire system.

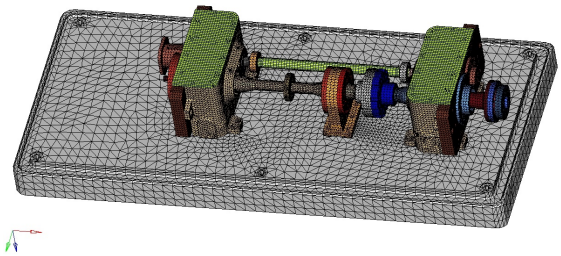

Figure 7: The FEM model of the investigated, statically overdetermined gearbox.

3D solid elements were used for the meshing, with three DOFs (displacements) in each node. The material properties of all the parts in the system are defined as steel with an elastic modulus $E = 210\,\mathrm{GPa}$. As a damping model we used the Hysteretic damping model with a 4 % loss factor for the entire system. In general, real systems dissipate energy, while vibrating, by several mechanisms. However, different damping mechanisms connected with localised damping issues are beyond the scope of this investigation.

The focus of our investigation is the bearings and their load-dependent stiffness. Therefore, it is crucial to determine how the bearings are modelled. The bearing inner and outer rings are modelled with second-order tetrahedral elements (see Figure 8). The rolling elements are not modelled as individual parts, since we would need to know the proper load zone and, consequently, have a very fine mesh on the rolling elements, as well as on both raceways. Besides that, the contact zone is changing nonlinearly with the load applied on it. The nonlinear contact issues between the rolling elements and the raceways exceed the FEM's capabilities. Thus, we calculate the bearing-stiffness matrix analytically (as described in Section 2) and position it in the FEM model between the inner and outer rings of the bearing. Each raceway groove is connected with a special element into one central (master) node, which represents a weighted average of the motions at a set of other (slave) grid points (corresponding raceway). Another element connects both master nodes (representing the inner and outer ring raceways) and defines the motion between them. The comprehensive bearing-stiffness matrix terms (Equation (9)) are prescribed as a property between both central master nodes. In such a way, the stiffness of each bearing is prescribed. In order to know the proper bearing-stiffness matrix, we have to know the load applied on it.

The load on the bearings was inserted into our system with a special clutch, where the torque was

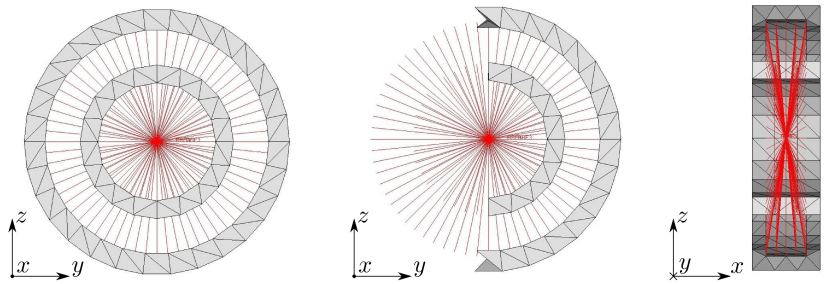

Figure 8: Roller bearing inner and outer ring with adjoining elements (left), cut view (middle) and section view (right).

generated. Figure 9 shows how the torque is applied in the FEM model. Both parts of the clutch (together with shafts w1 and w3) are shown as transparent, so we can see the applied load and the constraint. One part of the clutch is fixed in the rotational degree of freedom, whereas on the other one the torque is applied. The applied torque causes a deformation of the entire system (shaft bend and torsion, gear deflection, etc.) including the increased load on the bearings. After knowing the load on the bearings, we can calculate the corresponding bearing-stiffness matrix for each bearing (as described in Section 2). Since we do not know at the beginning either the bearing-stiffness matrices or the load applied to the bearings, an iterative process is needed to solve the problem. This process is described in detail in Section 6.

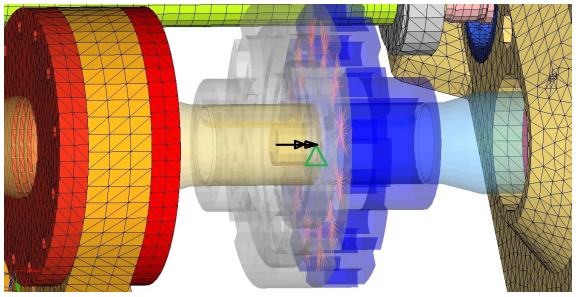

Figure 9: Applied static torque between shafts w1 and w3.

Two types of analyses are performed with the FEM model, i.e., the static analysis and the forced-response analysis. The former reflects the static behaviour of the gearbox after the torque is applied (new bearing mean loads) and the latter yields the dynamic properties of the gearbox for a given torque. It is important to note that the gearbox was never either measured or calculated under operational conditions.

6. Numerical solution – iterative process

As we have shown before, a statically overdetermined system that is supported by the bearings is impossible to solve analytically due to the number of unknown parameters. Therefore, an iterative process is needed. Figure 10 shows the overall data flow. One can see that two iterative processes are actually implemented, i.e., an inner iterative process and an outer iterative process. In Figure 10 they are both surrounded by a dashed line. Let us describe, step by step, every individual stage of the data flow.

The initial guess for each bearing mean-load vector is made first. We have found, that a very coarse assumption does not ruin the final solution. Normally, it only affects the speed of the convergence, but it does not change the final, converged values of the bearing mean-load vectors. This gives very positive feedback concerning the stability of the proposed solution. The initial guess for the bearing mean-load vector is inserted into the calculation of the bearing-stiffness matrix. Both the initial guess and the bearing-stiffness matrix calculation are performed separately for each bearing. For this reason they are surrounded with a dotted line. The calculation of the bearing-stiffness matrix represents the inner

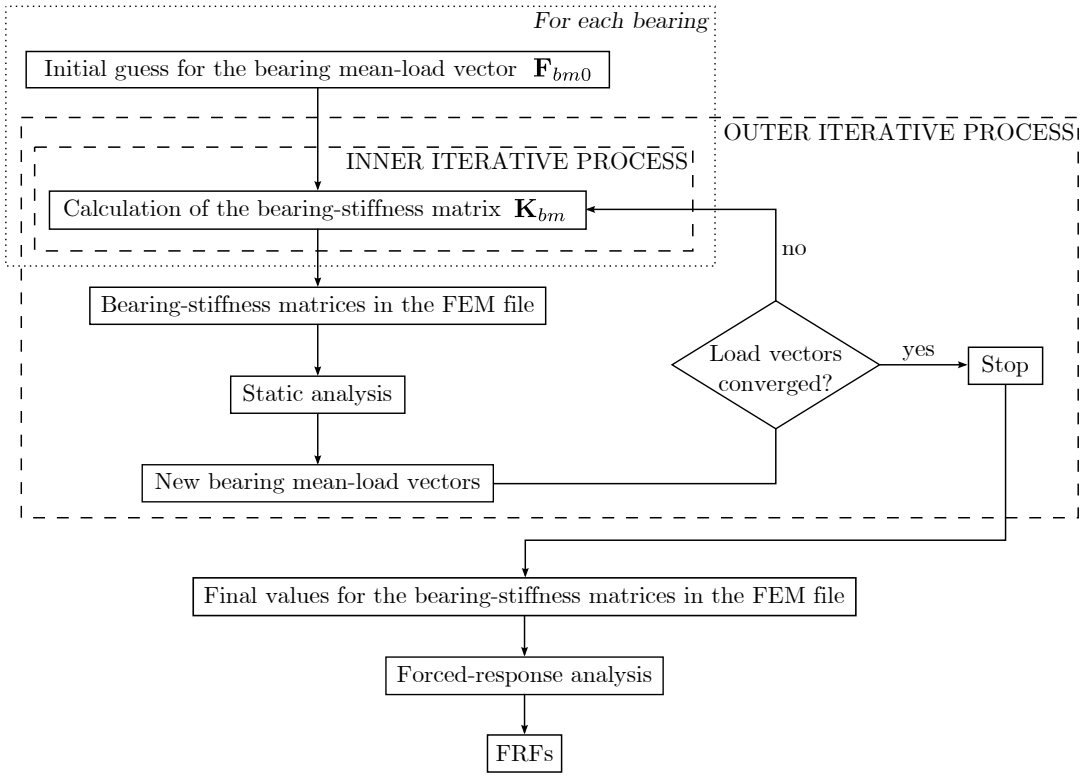

Figure 10: Data flow of the inner and outer iterative processes, together with final steps to obtain the FRFs.

iterative process, which contains more internal steps to provide the resulting bearing-stiffness matrix.

The basic steps of the inner iterative process are shown in Figure 11. Besides the bearing mean-load vector, an initial guess for the bearing mean-displacement vector also has to be provided. Choosing an appropriate initial guess for it requires a little more effort. The NRM is implemented to solve the obtained implicit set of nonlinear equations. The convergence and stability of the NRM is strongly affected by the initial guess. Basically, the initial guess for the bearing mean-displacement vector is connected with the orientation of the forces and the moments gathered in the bearing mean-load vector. This is necessary to consider in order to lead the calculation of the system of nonlinear equations to the proper (physically possible) solution and consequently to the correct bearing-stiffness matrix.

After the bearing-stiffness matrices for all the bearings are obtained, they are inserted into the FEM file. The next step is to calculate the static analysis with the applied torque preload on the place in the gearbox where the clutch is located. Four different torque preloads are investigated, 25 %, 50 %, 75 % and 100 % of the maximum torque preload. The higher the torque preload, the more loaded are the bearings. The results of the static analysis are new moments and forces (joined together in a bearing

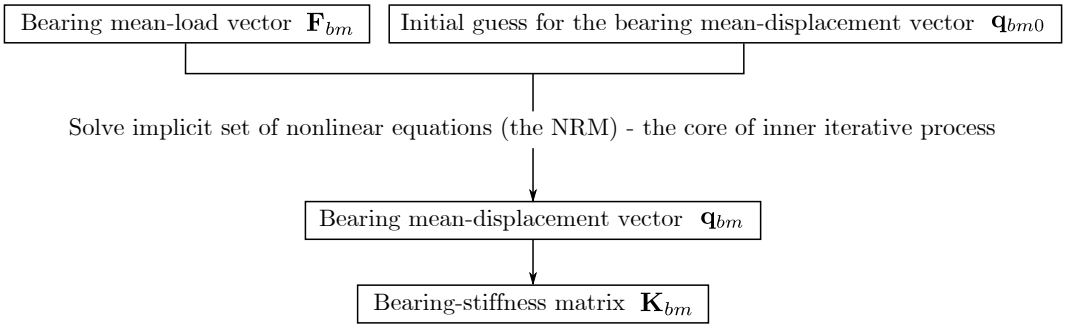

Figure 11: Basic steps of the inner iterative process, the output of which is the bearing-stiffness matrix.

mean-load vector for each bearing). If the newly obtained bearing mean-load vectors are not converged, compared to the last one computed, they are inserted as a new input into the bearing-stiffness matrix calculation. The described procedure runs until the bearing mean-load vectors are converged. At this level, we have reached the equilibrium state in our statically overdetermined gearbox, where the load vectors correspond to the proper bearing stiffness under the chosen torque preload. In the described procedure the flexibilities of all the other parts (shafts, housings, gears, etc.) are also taken into account, since the FEM model is used and the stiffness of each solid part is defined.

Together with the converged bearing mean-load vectors, the final bearing-stiffness matrices are also obtained for each of the applied torque preloads. It is important to note that separate analyses are performed for different torque preloads, i.e., the data flow described in Figure 10 is executed separately for each torque preload. Finally, the load dependency of the obtained FRFs can be investigated, to check the influence of the bearing-stiffness change on the vibration properties of the statically overdetermined gearbox. The comparison with the experimentally obtained FRFs is of great interest.

The data flow in Figure 10 represents a considerable amount of data handling and manipulation. Doing all the steps manually is much too time consuming and not acceptable at all, so the automation of the data flow is inevitable. Therefore, a code was written in order to automate the entire procedure. Finally, an initial guess for the bearing mean-load vectors has to be given at the beginning of the proposed method and afterwards the FRFs are obtained.

7. Experimental work

The experimental part of our investigation consists of measurements of the FRFs between different parts of the investigated gearbox. To show the influence of the bearing stiffness on the vibration properties, we investigated FRFs between the parts where the bearing stiffness has a significant influence on the transfer path. However, the bearing stiffness will effect every FRF, but the one between the housing and the shaft, or from one to another housing, will be affected more, due to the inevitable vibration transmission through the bearings. Figure 12 shows the three chosen points. Position one, marked with the white square, represents the hammer-excitation point. Positions two and three, marked with red squares, represent the placements for the accelerometers. Two transfer paths have been investigated, as is clear from Figure 12, where they are indicated with blue curves. Both FRFs are obtained from the excitation of the structure on the top lid of the transmission gearbox (point one), while measuring the acceleration on the top lid of the test gearbox (point two) and on the shaft (point three). We called the transfer path from point one to point two as the transfer path A and from point one to point three as the transfer path B. It is important to note that the hammer excitation is performed in the same direction as the accelerometers are measuring, i.e., in the z-direction.

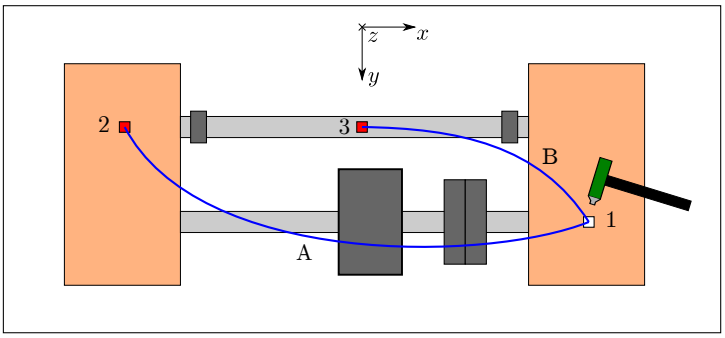

Figure 12: Test bench with enumerated points between which the FRFs have been obtained, together with the marked transfer paths.

The experimental workflow is shown in Figure 13. First, the torque preload is applied in the system, i.e., 25%, 50%, 75% and 100% of the maximum torque preload, which is equal to 218.2 N m. Special pliers are used to insert the desired torque preload, as shown in Figure 14. Strain gauges are mounted on the shaft w1 to help us define the appropriate value of the applied torque. After the torque preload is applied, the clutch is fixed with bolts and the impact excitation with the hammer at point one is conducted. It is important to note that the gearbox is not rotating while performing the measurements; it is just loaded with a static torque preload. The impact excitation causes an impact disturbance and

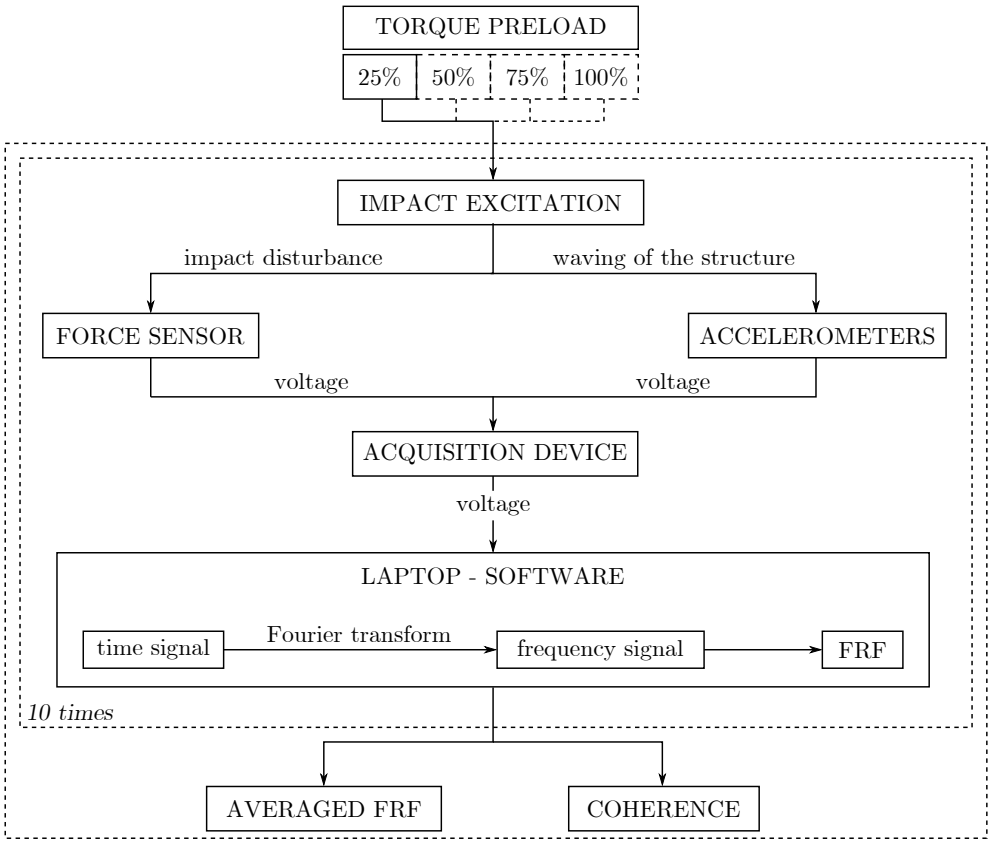

Figure 13: Experimental workflow.

the waving of the entire structure. The former is measured with the force sensor on the hammer tip and the latter with the accelerometers on points two and three. After this the acquisition device captures the signals and forwards them to a computer. The signal processing is performed and the time signals are converted with a Fourier transform into the frequency domain. The dynamic properties in the frequency domain are expressed as the accelerance [24]. The procedure is repeated ten times. After that, the averaged FRFs for the transfer paths A and B are obtained, together with the coherence, which serves as a criterion for the level of linearity and the quality of the performed measurements. During this step we have finished with one torque preload and we move to another and repeat the entire procedure, as is clearly shown in Figure 13. Finally, four different FRFs are obtained for both transfer paths. The changes in the FRFs between different torque preloads are of particular interest because they reflect the nonlinear bearing-stiffness change, which is caused by the applied torque preload.

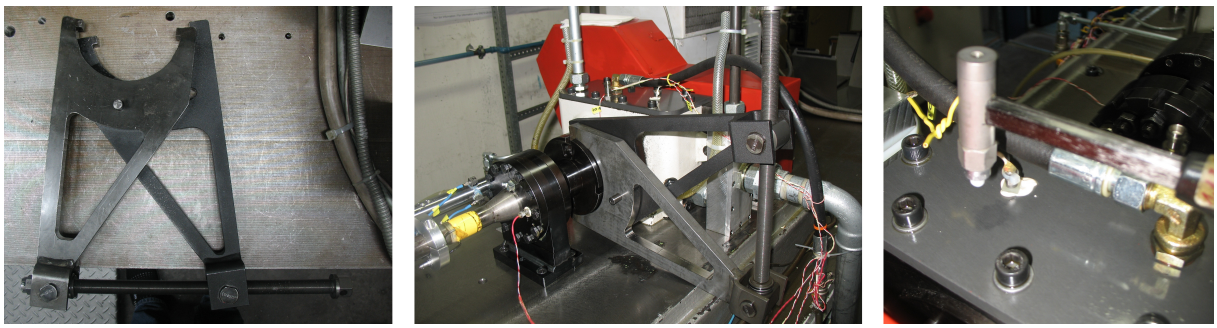

Figure 14: Special pliers to apply the torque preload (left) and their usage (middle). Impact excitation with a hammer on the top lid of the transmission gearbox (right).

8. Results

The entire data flow, presented in Figure 10, was executed for each torque preload, as described in Section 6. For each loop of the outer iterative process the load vectors are stored. At the end we can plot the convergence of the load-vector components for each bearing. It is important to note the coordinate system used, which was presented in Figure 6. Concerning the bearing distribution in our gearbox (see Figure 6), it is to be expected that convergence will be the most difficult to achieve on the bearings, where four of them are supporting the gear nearby and therefore seriously represent a statically overdetermined system. With respect to the last statement, all the bearings on the shaft w2 are included. Indeed, the convergence of the load vector is the worst on these bearings; however, it is still within reasonable limits, as presented in Figure 15 for bearing C_{w2}. The number of iterations N is equal to 200. It is clear that the fluctuations of the load-vector components never really disappear, but they can be reduced numerically with a weighting factor incorporated into the outer iterative process.

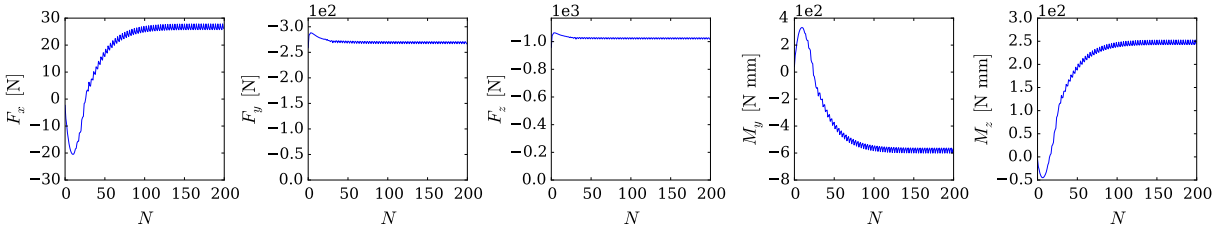

Figure 15: Convergence of the load-vector components, acting on the bearing C_{w2}, for a calculation with 100% of the maximum torque preload applied.

After the convergence is reached, we can plot the load-vector components for each bearing together, as shown in Figure 16. Such a presentation is much clearer and gives an overall insight into the load distribution on the bearings. Based on this presentation, the comparison of the load between the bearings can be made. The three different background colours represent the three different shafts: light blue, light green and light yellow correspond to w1, w2 and w3, respectively. It is important to note that the forces in all three directions are, in sum, equal to zero. The same does not apply to the moments. The reason for that lies in the roller bearings (A_{w1} and B_{w1}), which cannot carry an axial load. Consequently, these two bearings do not carry any moment, while the bearings A_{w3} and B_{w3} are fully loaded. The other parts of the gearbox have to compensate for the moment equilibrium in the system.

Finally, the FRFs for each torque preload are numerically obtained, taking into account the corresponding converged bearing-stiffness matrices. The FRFs are presented as Accelerance on a decibel scale with respect to the reference value being equal to one. Figure 17 shows the measured load dependency of the FRFs for the transfer path A and Figure 18 presents the calculated load dependency of the FRFs for the same transfer path. The situation is the same for transfer path B with Figures 19 and 20. The labels in the graphs consist of three parts. The first signifies the transfer path, the second part (letter) is for the type of obtained data ("m" for measurements and "s" for simulations) and the third is the percentage of the maximum torque preload applied. A similar load dependency behaviour is exhibited in the measured and simulated FRFs for both transfer paths. The bearing stiffness is a function of the load applied on it; therefore, the load dependency is of great interest and a crucial factor to rely on when evaluating the calculated FRFs. The load dependency is not really significant in the measured FRFs; however, we can see that the calculated load dependency is similar. The shapes of the curves do not move significantly relative to each other while changing the applied torque preload, what gives positive feedback for the bearing model and for the proposed algorithm.

Comparing the measured and simulated FRFs is the next step. If we take the measured and simulated FRFs of 100% of the maximum torque preload, Figure 21 shows the matching between them for the transfer path A and Figure 22 for the transfer path B. Compared to the appropriate description for load dependency, the matching between individual curves is not so good any more. Let us evaluate the calculated FRFs based on two criteria, i.e., the resonance peak positions and the amplitudes. The resonance peak positions are, in general, not very well predicted. However, some peaks are covered correctly, for example, at a frequency of 1050 Hz and 1500 Hz for both transfer paths and especially the two peaks at frequencies of 450 Hz and 550 Hz for the transfer path B. Also, other areas are partially well predicted in terms of resonance peak positions, e.g., at 370 Hz for both transfer paths and 2900 Hz

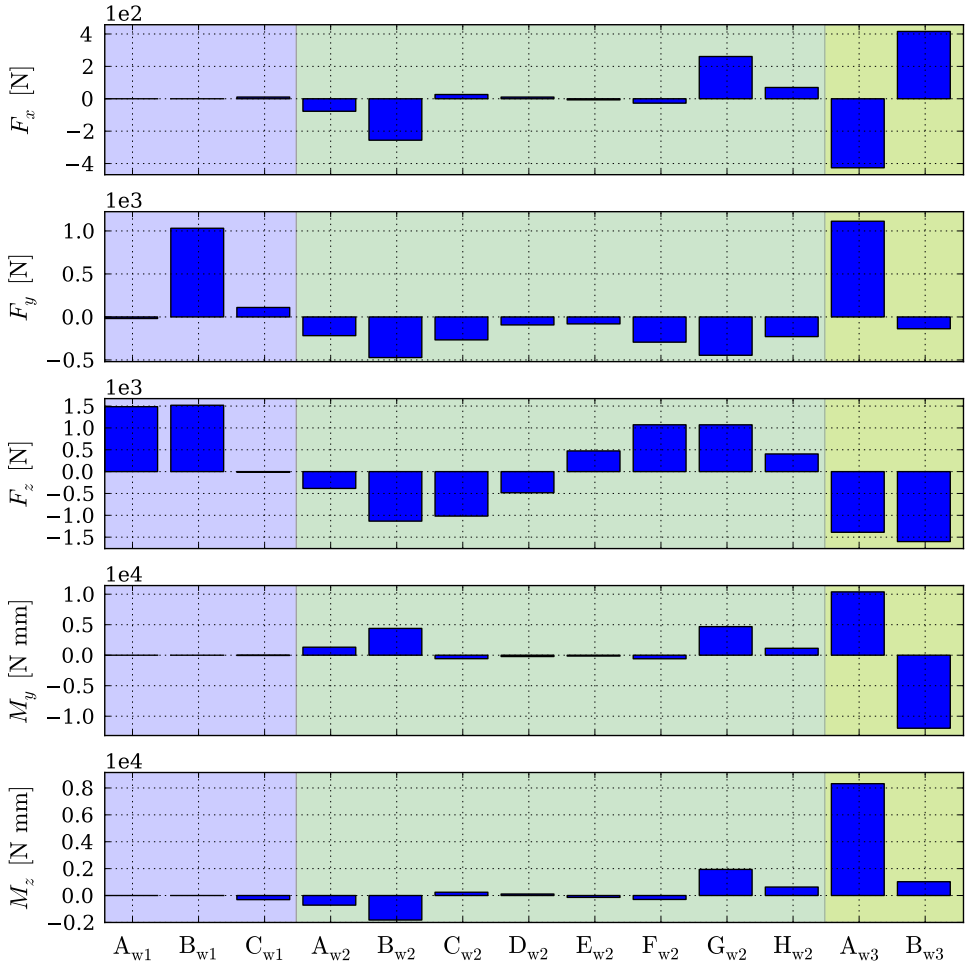

Figure 16: Amplitudes of the load-vector components, acting on each bearing in our gearbox, under 100% of the maximum torque preload.

for transfer path A; however, it is not possible to make a general conclusion about other regions. It is important to note the modes at the aforementioned eigenfrequencies. Figure 23 shows the modes for six different eigenfrequencies, that correspond to the well-predicted peaks in the spectra. Those peaks represent the modes of the shafts that are supported by the bearings. If the bearing stiffnesses change, the boundary conditions for the shafts (and also the housings) change, which is reflected in the different eigenfrequencies of the shafts and, consequently, of the entire gearbox. Therefore, the eigenfrequencies and the associated presented modes are significantly influenced by the bearing stiffnesses.

The amplitudes criterion evaluates the FRFs based on the amplitude discrepancies between the simulated and measured results. In general, the frequency range from 200 Hz up to 800 Hz, exhibits a better criterion satisfaction. However, for the transfer path B a better correlation is reached across the entire frequency range investigated. It is in general assumed that the FEM calculations can predict well the low-frequency response of a vibro-acoustic problem; however, it is not so in our case. The reason lies in the bad coherence of the measurements under 200 Hz and in the boundary conditions prescribed in the FEM model. The former results from an inability to apply stronger impact excitation and the latter results from the unknown clamping force of the supporting plate. It is important to note that the calculated amplitudes do not fit so well to the measured ones also due to the coarse assumption of general hysteretic damping model, applied for the entire gearbox.

The reasons for the discrepancies between the measured and calculated FRFs can be divided into two main groups: the bearing model and the FEM model with the associated parameters. Regarding the bearing model, the main issue is the Hertzian theory and the corresponding rolling-element, load-deflection, stiffness constant K_n. The mentioned value is a function of the bearing's inner geometry and

the material properties. These data are not only trade secrets of the bearing manufacturer, but also statistically distributed, which influences the calculation of the bearing-stiffness matrix. The other group of errors lies in the FEM model. Meshing details, different damping models, contact issues, etc. are the areas that are connected to the FEM modeling, but are beyond the scope of this investigation.

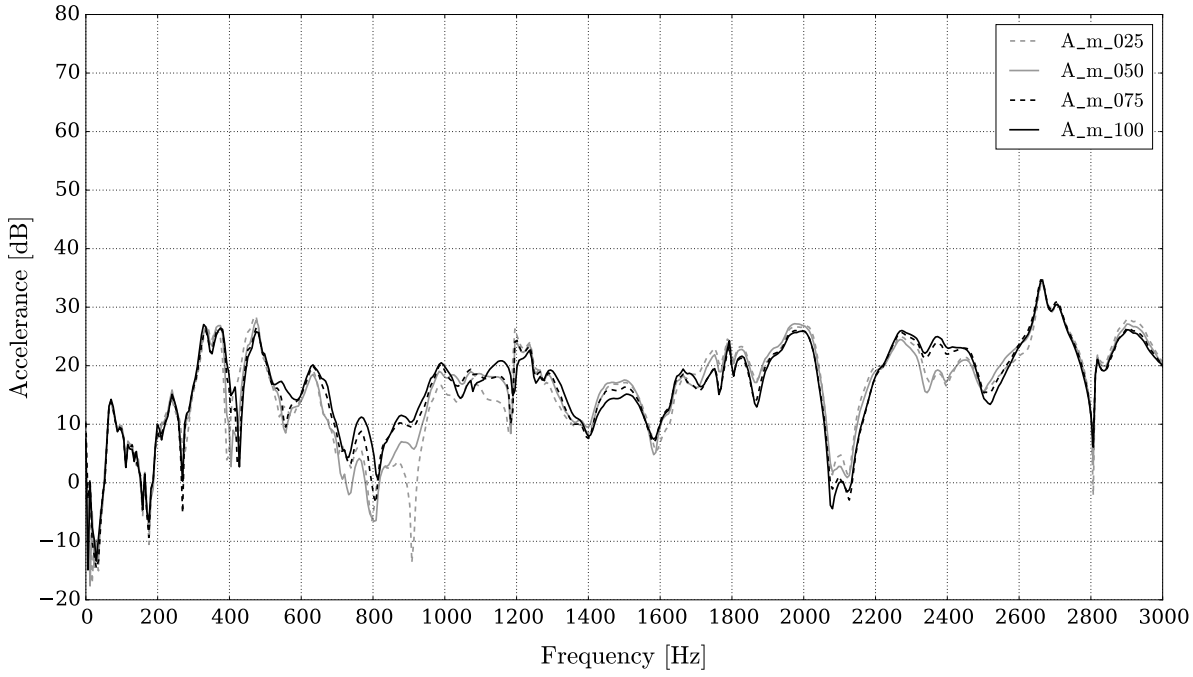

Figure 17: Load dependency of the measured FRFs for the transfer function A.

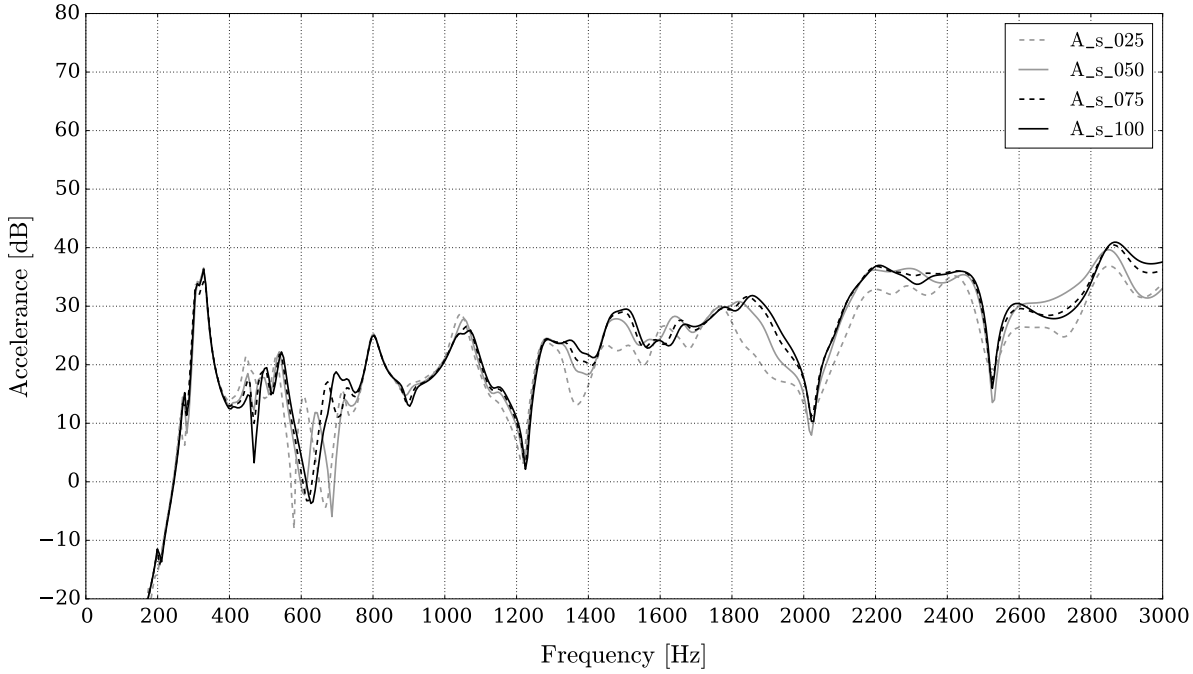

Figure 18: Load dependency of the calculated FRFs for the transfer function A.

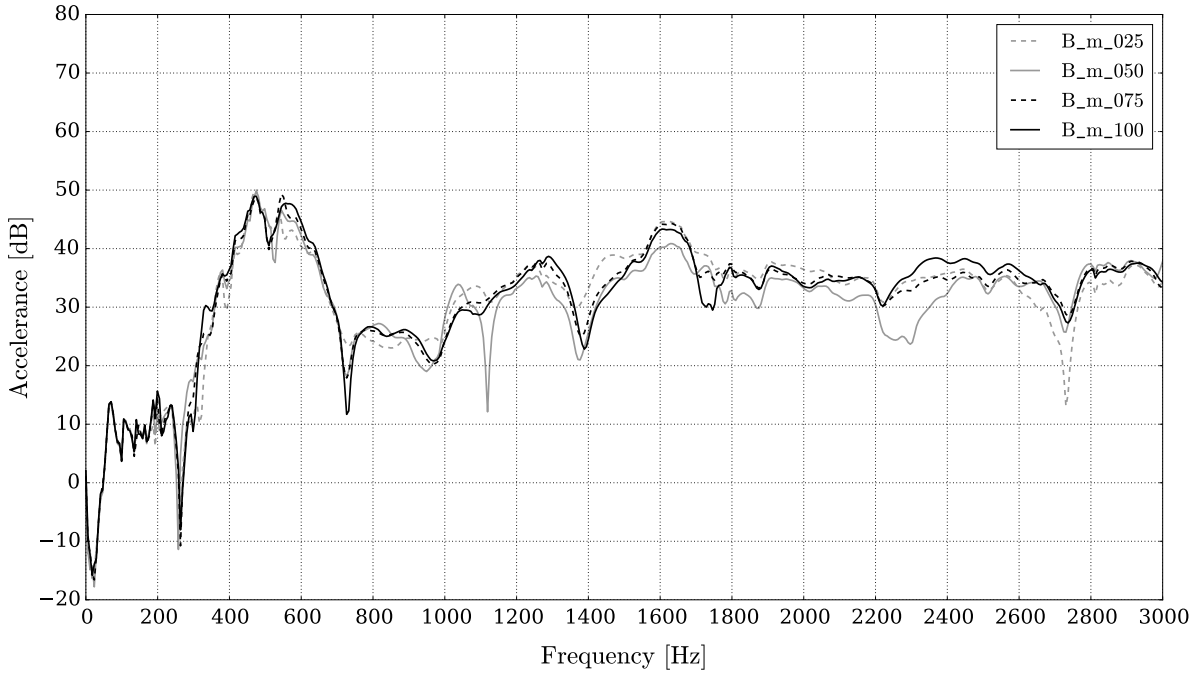

Figure 19: Load dependency of the measured FRFs for the transfer function B.

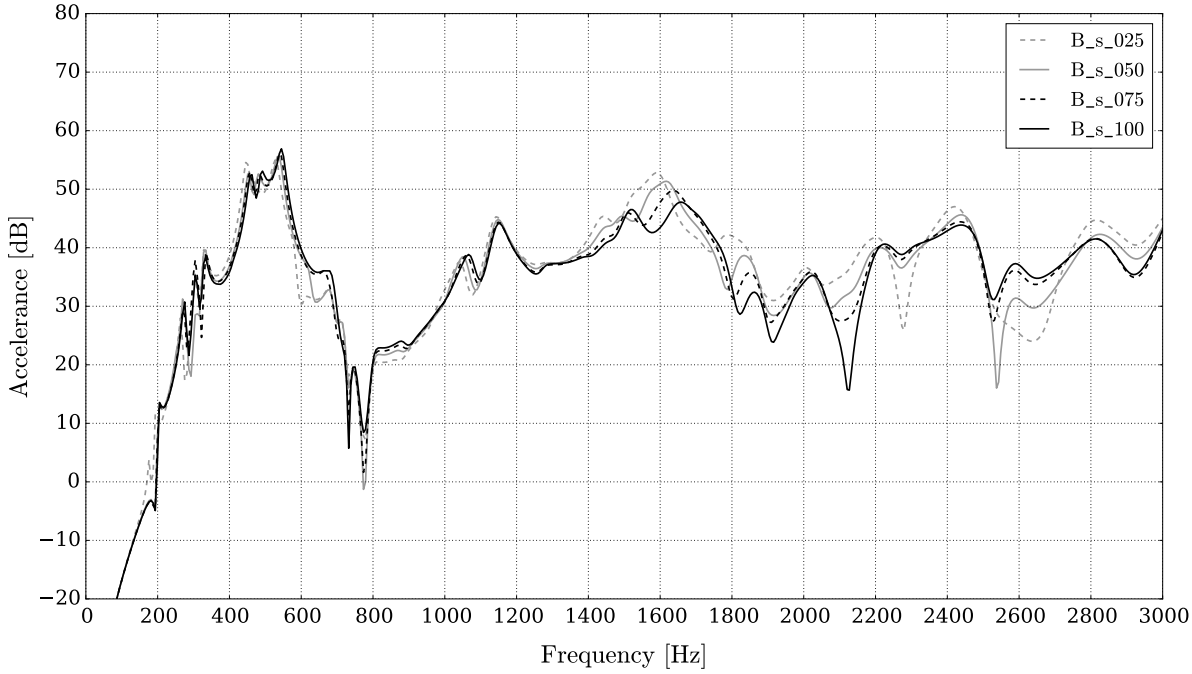

Figure 20: Load dependency of the calculated FRFs for the transfer function B.

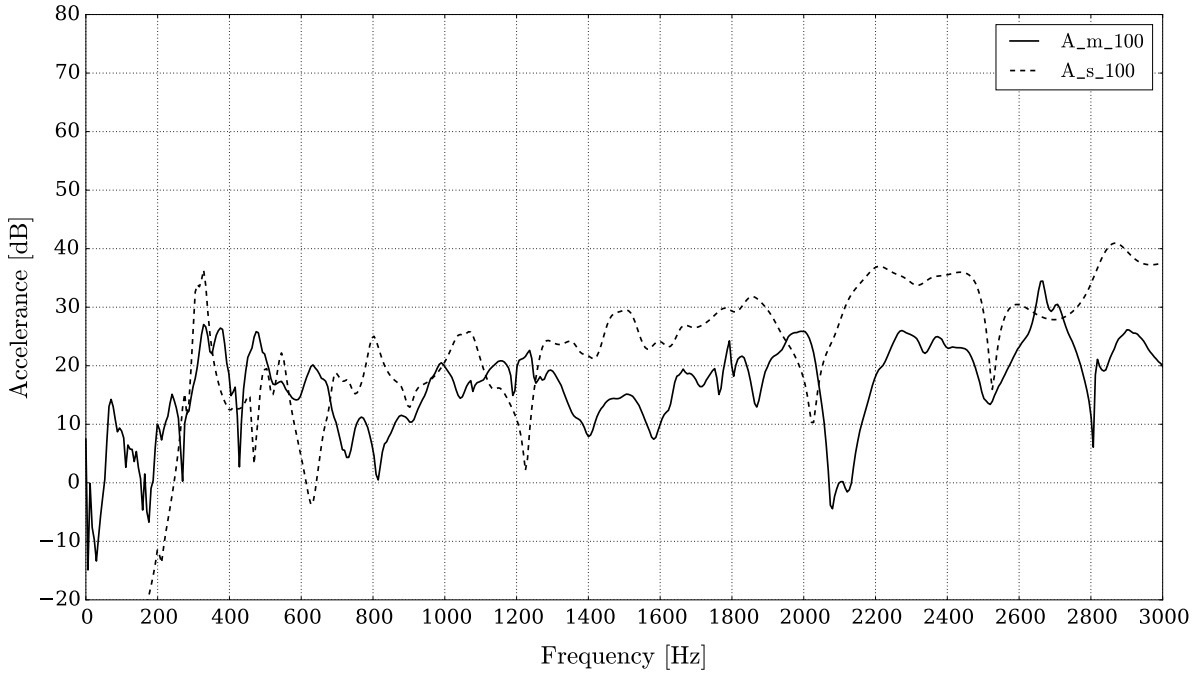

Figure 21: Comparison between the calculated and measured FRFs for the transfer function A. The load applied is 100% of the maximum torque preload.

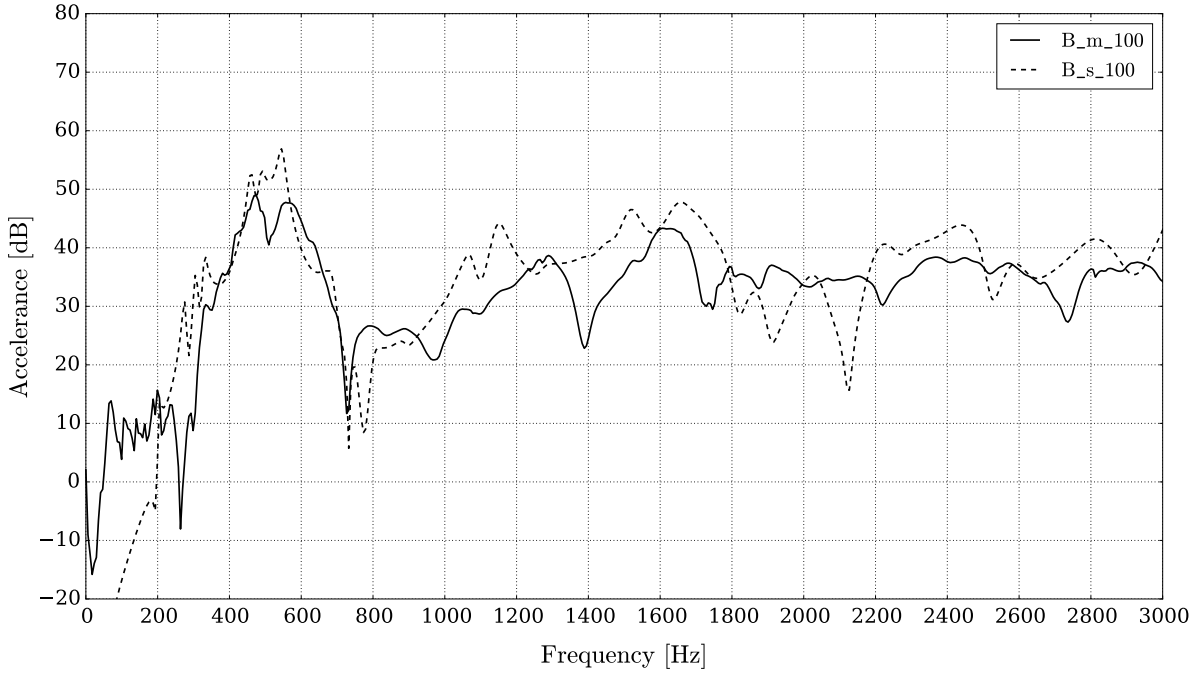

Figure 22: Comparison between the calculated and measured FRFs for the transfer function B. The load applied is 100% of the maximum torque preload.

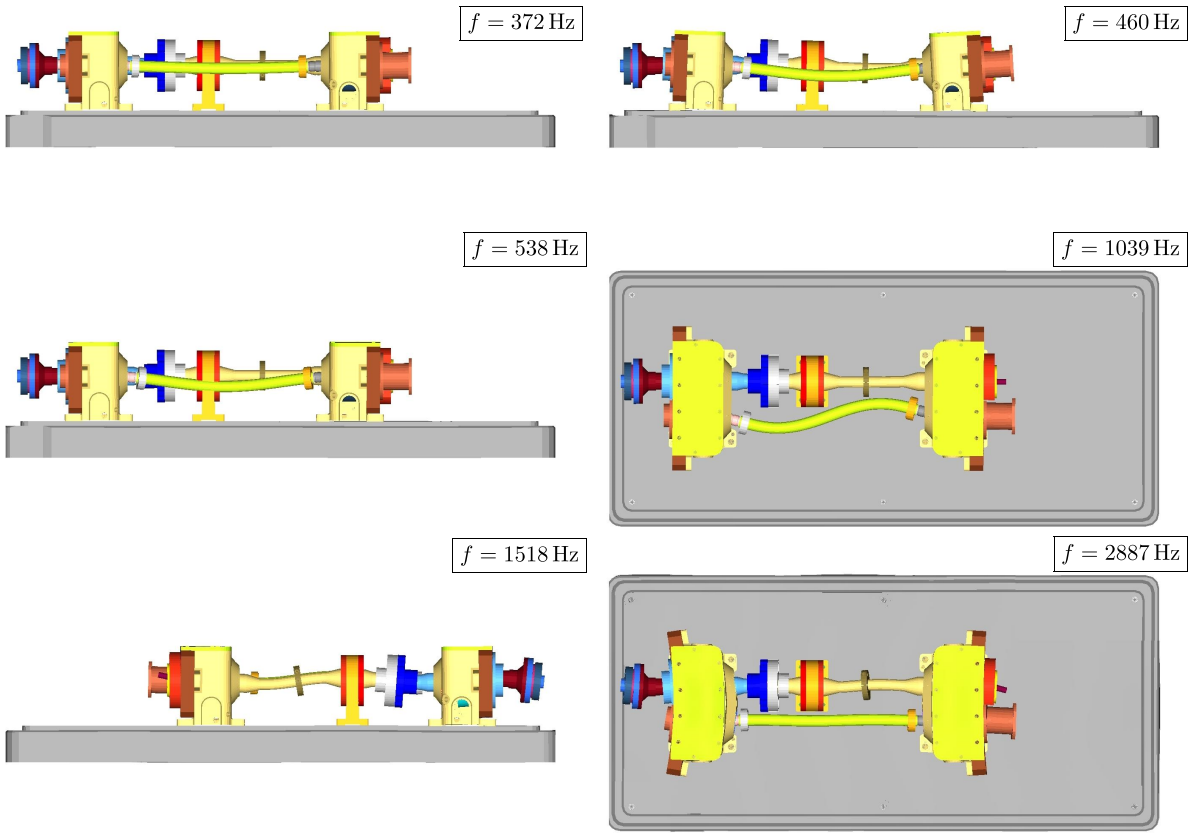

Figure 23: The modes of six different eigenfrequencies. Axial mode of the shaft w2 (top left), bending mode of the shaft w2 (top right, both in the middle), bending mode of the shafts w1, w2 and w3 (bottom left) and bending mode of the shafts w1 and w2, together with both housings (bottom right).

9. Conclusions

A new method for defining the bearing stiffness of statically overdetermined gearboxes was presented. First, a mathematical model is described, together with an explanation of the problem of static overdetermination. Second, an iterative process is introduced, programmed and automated in order to achieve the correct load on the bearings. This is necessary to obtain the proper bearing-stiffness matrices. After the correct bearing-stiffness matrices are obtained, the FRFs are calculated. Third, measurements of the FRFs are performed on a chosen statically overdetermined test-bench gearbox. Finally, the calculated FRFs are compared with the measured ones. The load dependency matches very well, giving a positive feedback to the proposed method.

Acknowledgements

We wish to thank the ZF company for supporting this research.

References

[1] J. Rao, Rotor dynamics, John Wiley, New york, 1983.

[2] H. Ozguven, On the critical speed of continuous shaft-disk systems, Journal of Sound and Vibration 106 (1984) 59–61.

[3] M. White, Rolling element bearing vibration transfer characteristics: Effect of stiffness, Journal of Applied Mechanics 46 (1979) 677–684.

[4] E. Gargiulo, A simple way to estimate bearing stiffness, Machine design 52 (1980) 107–110.

[5] T. Harris, Rolling bearing analysis, John Wiley, New york, 1984.

[6] E. Krämer, Dynamics of Rotors and Foundations, Springer, Berlin, 1993.
[7] T. Lim, R. Singh, Vibration transmission through rolling element bearings, part 1: bearing stiffness formulation, Journal of Sound and Vibration 139 (2) (1990) 179–199.
[8] T. Royston, I. Basdogan, Vibration transmission through self-aligning (spherical) rolling element bearings: Theory and experiment, Journal of Sound and Vibration 215(5) (1998) 997–1014.
[9] T. Lim, R. Singh, Vibration transmission through rolling element bearings, part 3: geared rotor system studies, Journal of Sound and Vibration 152 (1) (1991) 31–54.
[10] T. Lim, R. Singh, Vibration transmission through rolling element bearings, part 4: statistical energy analysis, Journal of Sound and Vibration 153 (1) (1992) 37–50.
[11] P. Čermelj, M. Boltežar, An indirect approach to investigating the dynamics of a structure containing ball bearings, Journal of Sound and Vibration 276 (2004) 401–417.
[12] H. Liew, T. Lim, Analysis of time-varying rolling element bearing characteristics, Journal of Sound and Vibration 283 (2005) 1163–1179.
[13] A. Gunduz, J. Dreyer, R. Singh, Effect of bearing preloads on the modal characteristics of a shat-bearing assembly: Experiments on double row angular contact ball bearings, Mechanical Systems and Signal Processing 31 (2012) 176–195.
[14] Y.Guo, R. Parker, Stiffness matrix calculation of rolling element bearings using a finite element/contact mechanics model, Mechanism and Machine Theory 51 (2012) 32–45.
[15] S. Vijayakar, A combined surface integral and finite element solution for a three-dimensional contact problem, International Journal for Numerical Methods in Engineering 31 (1991) 524–546.
[16] X. Sheng, B. Li, Z. Wu, H. Li, Calculation of ball bearing speed-varying stiffness, Mechanisms and Machine Theory 81 (2014) 166–180.
[17] J. Kraus, J. Blech, S. Braun, In situ determination of rolling bearing stiffness and damping by modal analysis, Journal of Vibration, Acoustics, Stress, and Reliability in Design 109 (1987) 235–240.
[18] T. Lim, R. Singh, Vibration transmission through rolling element bearings, part 2: system studies, Journal of Sound and Vibration 139 (2) (1990) 201–225.
[19] S. Spiewak, T. Nickel, Vibration based preload estimation in machine tool spindles, Journal of Machine Tools and Manufacture 41 (2001) 567–588.
[20] D. Lee, D. Choi, A dynamic analysis of a flexible rotor in ball bearings with nonlinear stiffness characteristics, International Journal of Rotating Machinery 3 (1997) 73–80.
[21] W. Jacobs, R. Boonen, P. Sas, D. Moens, The influence of the lubricant film on the stiffness and damping characteristics of a deep groove ball bearing, Mechanical Systems and Signal Processing 42 (2014) 335–350.
[22] Y. Guo, T. Eritenel, T. Ericson, R. Parker, Vibro-acoustic propagation of gear dynamics in a gear-bearing-housing system, Journal of Sound and Vibration 333 (2014) 5762–5785.
[23] W. Hu, N. Feng, E. Hahn, A comparison of techniques for identifying the configuration state of statically indeterminate rotor bearing systems, Tribology International 37 (2004) 149–157.
[24] N. M. M. Maia, J. M. M. Silva, Theoretical and Experimental Modal Analysis, Research Studies Press Ltd., 1997.